

Saturation of MRI via parasitic modes

Martin E. Pessah^{1,2}

¹ Niels Bohr International Academy
Niels Bohr Institute, University of Copenhagen
Blegdamsvej 17, 2100, Copenhagen, Denmark

²Institute for Advanced Study
Einstein Drive, Princeton, NJ, 08540, USA
email: mpessah@nbi.dk

Abstract. Understanding the physical mechanisms that play a role in the saturation of the magnetorotational instability (MRI) has been an outstanding problem in accretion physics since the early 90's. Here, we present the summary of a study of the parasitic modes that feed off exact viscous, resistive MRI modes. We focus on the situation in which the amplitude of the magnetic field produced by the MRI is such that the instantaneous growth rate of the fastest parasitic mode matches that of the fastest MRI mode. We argue that this "saturation" amplitude provides an estimate of the magnetic field that can be generated by the MRI before the secondary instabilities suppress its growth significantly. We show that there exist two regimes, delimited by a critical Elsasser number of order unity, in which saturation is achieved via secondary instabilities that correspond to either Kelvin-Helmholtz or tearing modes.

Keywords. accretion, accretion disks, magnetohydrodynamics, instabilities, turbulence

1. Introduction

Let us consider a homogeneous, incompressible plasma in differential rotation according to $\boldsymbol{\Omega} = \Omega(r)\hat{\mathbf{z}}$ and threaded by a vertical magnetic field $\mathbf{B} = B_z\hat{\mathbf{z}}$. The equations governing the local dynamics of this MHD fluid in the shearing box approximation are

$$\frac{\partial \mathbf{v}}{\partial t} + (\mathbf{v} \cdot \nabla) \mathbf{v} = -2\boldsymbol{\Omega} \times \mathbf{v} + q\Omega_0^2 \nabla(r - r_0)^2 - \frac{1}{\rho} \nabla \left(P + \frac{\mathbf{B}^2}{8\pi} \right) + \frac{(\mathbf{B} \cdot \nabla) \mathbf{B}}{4\pi\rho} + \nu \nabla^2 \mathbf{v}, \quad (1.1)$$

$$\frac{\partial \mathbf{B}}{\partial t} + (\mathbf{v} \cdot \nabla) \mathbf{B} = (\mathbf{B} \cdot \nabla) \mathbf{v} + \eta \nabla^2 \mathbf{B}, \quad \text{with } \nabla \cdot \mathbf{B} = 0 \quad \text{and} \quad \nabla \cdot \mathbf{v} = 0. \quad (1.2)$$

Here, P is the pressure, ρ is the density, and the factor $q \equiv -d \ln \Omega / d \ln r$ parametrizes the magnitude of the local shear; $q = 3/2$ in the Keplerian case. Non-ideal effects due to a constant kinematic viscosity and resistivity are included in the terms proportional to ν and η . We work with dimensionless variables defined in terms of the background Alfvén speed and the local angular frequency and define the numbers $\Lambda_\nu \equiv \bar{v}_{Az}^2 / \nu \Omega_0$ and $\Lambda_\eta \equiv \bar{v}_{Az}^2 / \eta \Omega_0$, whose ratio is the magnetic Prandtl number, $\text{Pm} \equiv \nu / \eta \equiv \Lambda_\eta / \Lambda_\nu$. The quantity Λ_η is known as the Elsasser number, while Λ_ν stands for its viscous counterpart.

The exact equations for the evolution of the secondary instabilities $\delta \mathbf{v}(\mathbf{x}, t)$ and $\delta \mathbf{B}(\mathbf{x}, t)$ affecting an MRI mode are obtained by substituting in Equations (1.1) and (1.2) the ansatz $\mathbf{v} = -q\Omega_0(r - r_0)\hat{\boldsymbol{\phi}} + \Delta \mathbf{v} e^{\Gamma t} + \delta \mathbf{v}$ and $\mathbf{B} = B_z\hat{\mathbf{z}} + \Delta \mathbf{B} e^{\Gamma t} + \delta \mathbf{B}$. The first term in each of these equations accounts for the background Keplerian velocity and magnetic field. The terms proportional to $\Delta \mathbf{v} \equiv \mathbf{V}_0 \sin(Kz)$ and $\Delta \mathbf{B} \equiv \mathbf{B}_0 \cos(Kz)$ correspond to the exact, exponential fluctuations due to the MRI (Balbus & Hawley 1991), and $\Gamma(\nu, \eta, K)$ is the growth rate of the unstable MRI mode with wavelength $\lambda = 2\pi/K$ (see

Pessah & Chan 2008 for details). This substitution leads to partial differential equations for $\delta\mathbf{v}(\mathbf{x}, t)$ and $\delta\mathbf{B}(\mathbf{x}, t)$. However, we can gain insight into the growth rates and physical properties of the secondary instabilities by assuming that the exact (primary) MRI modes can be considered as a time-independent background from which the (secondary) parasitic modes feed off (see, e.g., Goodman & Xu 1994, Pessah & Goodman 2009, Latter *et al.* 2009, and Pessah 2010 for more details about this approach). In this framework, the dynamics of the parasitic modes is determined by

$$[(s + \nu(k_h^2 - \partial_z^2))(k_h^2 - \partial_z^2)\delta v_z - i(\mathbf{k}_h \cdot \Delta\mathbf{v})(k_h^2 - \partial_z^2 - K^2)\delta v_z + i(\mathbf{k}_h \cdot \Delta\mathbf{B})(k_h^2 - \partial_z^2 - K^2)\delta B_z = 0, \tag{1.3}$$

$$[s + \eta(k_h^2 - \partial_z^2)]\delta B_z + i(\mathbf{k}_h \cdot \Delta\mathbf{B})\delta v_z - i(\mathbf{k}_h \cdot \Delta\mathbf{v})\delta B_z = 0. \tag{1.4}$$

Here, as in Goodman & Xu (1994), we have further neglected the influence of the weak vertical background field, the Coriolis force, and the background shear flow on the dynamics of the secondary modes. The wavenumber k_h is the modulus of the horizontal wavevector $\mathbf{k}_h \equiv k_x\hat{x} + k_y\hat{y} \equiv k_h(\cos\theta\hat{x} + \sin\theta\hat{y})$ associated with the parasites.

2. Parasitic Modes

Let us focus our attention on the stability of the fastest growing MRI modes, with $K = K_{\max}(\nu, \eta)$ and $\Gamma = \Gamma_{\max}(\nu, \eta)$, and let us further consider their fastest growing parasites. It is then possible to estimate the amplitude B_0^{sat} such that the fastest parasitic mode, for given values of Λ_ν and Λ_η , grows as fast as the primary mode upon which it feeds. The motivation to calculate this "saturation" amplitude is that the parasite will be able to drain an amount of energy of order $(B_0^{\text{sat}})^2$ from the primary mode shortly after their growth rates are comparable (see Pessah 2010 for more details).

The left panel of Fig. 1 shows the MRI saturation amplitude as a function of magnetic Prandtl number and the viscosity, while the right panel shows the dimensionless stress $\alpha_{\text{sat}}\beta_{\text{sat}} \equiv \bar{T}_{r\phi}/(B_0^2/8\pi)$. For $\Lambda_\nu \gtrsim 10$, the magnetic energy density presents two asymptotic regimes that correspond to Λ_η larger or smaller than unity. The associated modes correspond to Kelvin-Helmholtz and tearing modes respectively (see Fig. 2 and the discussion below). Note that in the limit $\Lambda_\nu, \text{Pm} \gg 1$, $\alpha_{\text{sat}}\beta_{\text{sat}} \rightarrow 0.4$, while in the inviscid, resistive limit, i.e., $\Lambda_\nu \gg 1$ and $\text{Pm} \ll 1$, $\alpha_{\text{sat}}\beta_{\text{sat}} \rightarrow 0.5\Lambda_\eta$. Thus, despite the

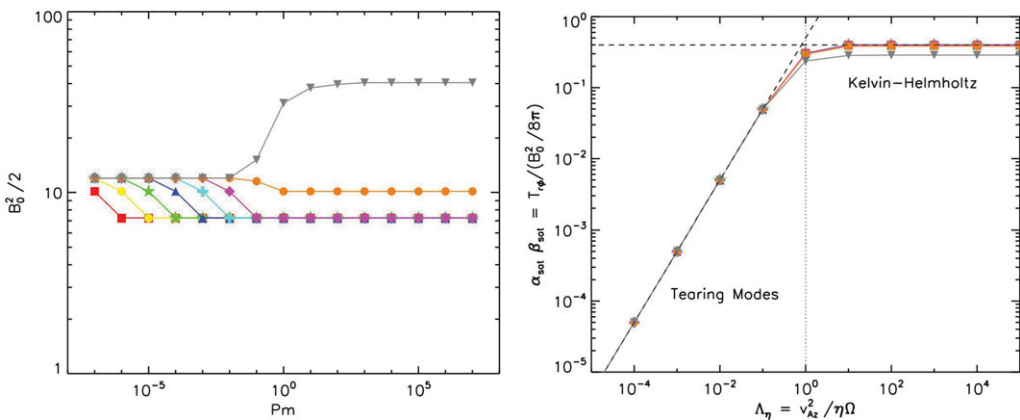


Figure 1. Predicted magnetic energy density (left) and dimensionless stress (right) for the fastest MRI mode if saturation occurs when the fastest parasitic mode matches its growth rate.

fact that the magnetic field at saturation asymptotes to a constant value, the dimensionless stress decreases linearly with Λ_η for $\Lambda_\eta \lesssim 1$. This is in qualitative agreement with the simulations in Sano & Stone (2002) (c.f., Pessah 2010; Longaretti & Lesur 2010).

In order to understand the nature of the fastest secondary modes it is useful to analyze their structure along the directions associated with their fastest growth, i.e., $\theta \equiv \theta_{\max}$. For fixed values of the dissipation coefficients, the growth rates of the secondary instabilities peak around directions which are almost aligned with either the velocity or magnetic fields of the primary MRI mode, i.e., $\theta_{\max} \simeq \theta_V$ for $\Lambda_\eta \gg 1$ and $\theta_{\max} \simeq \theta_B$ for $\Lambda_\eta \ll 1$. Fig. 2 shows the physical structure of the fastest parasitic modes, including the velocity and magnetic fields of the primary MRI modes, for $\Lambda_\eta = \{0.1, 1, 10\}$, from left to right, with $\Lambda_\nu \gg 1$. The arrows in the upper and lower panels correspond to the projections of the total (primary plus secondary) velocity and magnetic fields onto the plane defined by the z -axis and the direction θ_{\max} . The color contours correspond to the total vorticity and current density projected onto the direction perpendicular to θ_{\max} .

Tearing Modes — For the Elsasser number $\Lambda_\eta = 0.1$, the versor characterizing the direction of fastest growth, $\check{\mathbf{k}}_h$, points in the direction $\theta_{\max} \simeq \theta_B$. This mode, shown in the leftmost (upper and lower) panels of Fig. 2, feeds off the current density of the primary MRI mode. The current density of the secondary modes presents maxima and minima along the planes $z = \pm n\pi/2$ where the magnetic field of the primary mode, $\Delta \mathbf{B} = \mathbf{B}_0 \cos(Kz)$, reverses sign. Thus, the fluctuations induced by these fastest resistive secondary modes tend to promote reconnection of the MRI field. The observed mode structure is qualitatively insensitive to the value of the Elsasser number as long as $\Lambda_\eta < 1$ and $\Lambda_\nu \gg 1$. We thus conclude that the fastest parasitic modes correspond to tearing

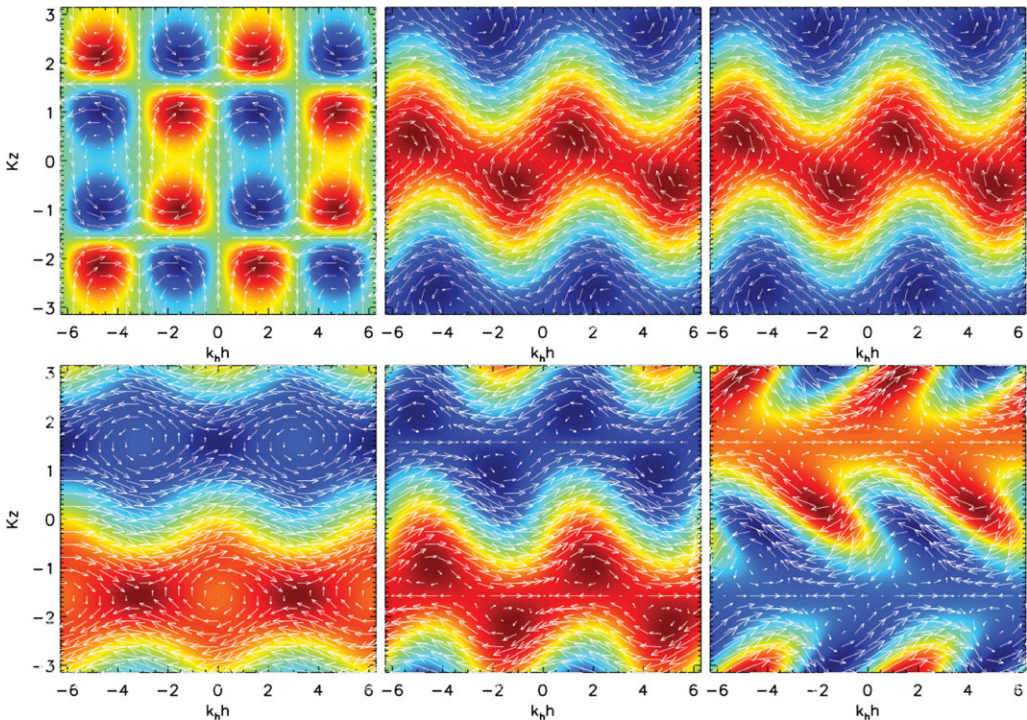


Figure 2. Physical structure of the fastest parasitic modes, including the velocity and magnetic fields of the primary modes, for $\Lambda_\eta = \{0.1, 1, 10\}$, from left to right, with $\Lambda_\nu \gg 1$.

modes for $\Lambda_\eta < 1$. These parasitic modes are enabled by non-zero resistivity and are thus absent in the ideal MHD regime studied by Goodman & Xu (1994).

Kelvin-Helmholtz Modes — The two rightmost sets of panels in Fig. 2 show the fastest secondary modes for the Elsasser numbers $\Lambda_\eta = \{1, 10\}$. The versors $\check{\mathbf{k}}_h$ characterizing the direction of fastest growth point in the direction $\theta_{\max} \simeq \theta_V$. These modes feed off the shear in the velocity field of the primary MRI modes. The velocity and vorticity fields show a periodic structure similar to what is obtained in the stability analysis of a periodic set of equidistant vortex sheets distributed along the $\check{\mathbf{z}}$ direction and alternating sense. The structure of these modes is quantitatively insensitive to the value of the Elsasser number as long as $\Lambda_\eta \geq 1$ and $\Lambda_\nu \gg 1$. We thus conclude that the fastest parasitic modes correspond to Kelvin-Helmholtz modes for $\Lambda_\eta > 1$. In the limit $\Lambda_\eta \gg 1$, these correspond to the Kelvin-Helmholtz modes alluded to in Goodman & Xu (1994).

3. Discussion

In order to solve for the dynamics of the parasitic modes we have made a number of assumptions which might affect the value of the saturation amplitudes presented here. Despite these limitations, the properties of the parasitic modes that we described provide valuable analytical guidance and a basic framework to design and interpret tailored numerical experiments of the nonlinear saturation of the MRI. The following is a summary of our findings[†]. When the magnetic fields involved are weak enough so that the incompressible limit holds, the parameter driving the behavior of the growth rates of the MRI and its parasites, and thus the magnetic energy density and stresses at saturation, is the Elsasser number Λ_η . In particular, we found that, as long as viscous dissipation is small, i.e., $\Lambda_\nu \gtrsim 10$, then there exists two regimes: (i) quasi-ideal MHD, where the physical properties of the MRI and its parasitic instabilities are insensitive to dissipation. This holds as long as $\Lambda_\eta > 1$, which is applicable to the fully ionized regions of accretion disks around compact objects. (ii) inviscid, resistive MHD, where all the relevant dependencies on Λ_ν and Pm are only through the product $\text{Pm} \Lambda_\nu$, i.e., the Elsasser number Λ_η . This regime corresponds to $\Lambda_\eta < 1$, and characterizes poorly ionized regions of protoplanetary disks. The Elsasser number for current Taylor-Couette MRI experiments is close to unity and thus both types of modes present similar growth rates in this regime.

References

- Balbus, S. A. & Hawley, J. F. 1991, *ApJ*, 376, 214
 Goodman, J. & Xu, G. 1994, *ApJ*, 432, 213
 Jamroz, B., Julien, K., & Knobloch, E. 2008, *PhST*, 132, 4027
 Latter, H. N., Lesaffre, P., & Balbus, S. A. 2009, *MNRAS*, 394, 715
 Longaretti, P. Y. & Lesur, G. 2010, *A&A*, 516, 51
 Pessah, M. E. & Chan, C. K. 2008, *ApJ*, 684, 498
 Pessah, M. E. & Goodman, J. 2009, *ApJ*, 698, L72
 Pessah, M. E. 2010, *ApJ*, 716, 1012
 Sano, T., Inutsuka, S. I., & Miyama, S. M. 1998, *ApJ*, 506, L57
 Sano, T. & Stone, J. M. 2002, *ApJ*, 577, 534
 Umurhan, O. M., Regev, O., & Menou, K. 2007, *Phys. Rev. E*, 76, 6310
 Vishniac, E. 2009, *ApJ*, 696, 1021

[†] For reasons of space, it is not possible to make justice to a number of different approaches addressing the saturation of the MRI. We refer the reader to the works by, e.g., Sano *et al.* (1998), Umurhan *et al.* (2007), Jamroz *et al.* (2008), Vishniac (2009), Latter *et al.* (2009), Longaretti & Lesur (2010), and the relevant references therein, for other perspectives into this problem.